UCRL- JC-103626
PREPRINT

CIRCULATION
SUBJECT TO RE
IN TWO WEE

SENSOR FUSION METHODOLOGY FOR REMOTE DETECTION OF BURIED LAND MINES

Nancy Del Grande
Lawrence Livermore National Laboratory
Livermore, CA 94550

This paper was prepared for the Proceedings of the
3rd National Symposium on Sensor Fusion,
Orlando, Florida
April 16-20, 1990

April 1990

Lawrence Livermore National Laboratory

This is a preprint of a paper intended for publication in a journal or proceedings. Since changes may be made before publication, this preprint is made available with the understanding that it will not be cited or reproduced without the permission of the author.

DISCLAIMER

This document was prepared as an account of work sponsored by an agency of the United States Government. Neither the United States Government nor the University of California nor any of their employees, makes any warranty, express or implied, or assumes any legal liability or responsibility for the accuracy, completeness, or usefulness of any information, apparatus, product, or process disclosed, or represents that its use would not infringe privately owned rights. Reference herein to any specific commercial products, process, or service by trade name, trademark, manufacturer, or otherwise, does not necessarily constitute or imply its endorsement recommendation, or favoring of the United States Government or the University of California. The views and opinions of authors expressed herein do not necessarily state or reflect those of the United States Government or the University of California, and shall not be used for advertising or product endorsement purposes.

SENSOR FUSION METHODOLOGY FOR REMOTE DETECTION OF BURIED LAND MINES

Nancy Del Grande
Lawrence Livermore National Laboratory
Livermore, CA 94550

ABSTRACT

We are investigating a sensor fusion methodology for remote detection of buried land mines. Our primary approach is sensor intrafusion. Our dual-channel passive IR methodology decouples true (corrected) surface temperature variations of 0.2°C from spatially dependent surface emissivity noise. It produces surface temperature maps showing patterns of conducted heat from buried objects which heat and cool differently from their surroundings. Our methodology exploits Planck's radiation law. It produces separate maps of surface emissivity variations which allow us to reduce false alarms. Our secondary approach is sensor interfusion using other methodologies. For example, an active IR CO_2 laser reflectance channel helps distinguish surface targets unrelated to buried land mines at night when photographic methods are ineffective. Also, the interfusion of ground penetrating radar provides depth information for confirming the site of buried objects. Together with EG&G in Las Vegas, we flew a mission at Nellis AFB using the Daedalus dual-channel (5 and 10 micron) IR scanner mounted on a helicopter platform at an elevation of 60 m above the desert sand. We detected surface temperature patterns associated with buried (inert) land mines covered by as much as 10 cm of dry sand. The respective spatial, spectral, thermal, emissivity and temporal signatures associated with buried targets differed from those associated with surface vegetation, rocks and manmade objects. Our results were consistent with predictions based on the annual Temperature Wave Model. They were confirmed by field measurements. The dual-channel sensor fusion methodology is expected to enhance the capabilities of the military and industrial community for standoff mine detection. Other important potential applications are open skies, drug traffic control and environmental restoration at waste burial sites.

1.0 BACKGROUND AND TECHNICAL APPROACH

The first successful application of the sensor intrafusion methodology which uses two passive IR channels was for geothermal resource investigations in 1977. Predawn surface temperature patterns were spatially correlated with sub-surface heat flow anomalies, soil moisture differences and variations in solar heat retained by near-surface rock outcrops.[1,2] A 2 square km aquifer was depicted by the corrected thermal imagery. The aquifer was less than 60 m deep. See Figure 1.

Other applications of the methodology were conducted at the Mercury Nevada Test Site for treaty verification. We investigated the surface temperature signatures near "ground zero" before and after an underground nuclear explosion. Soil "fluffing" changes the soil thermal diffusivity and consequently the heating and cooling properties of near-surface materials near "ground zero". All else being equal, the ground nearby has a different temperature variation with time than the ground further away.

Another application of the methodology provided a service for the archaeological community. Cabrillo College archaeologist Rob Edwards was planning to excavate an area with a suspected 200 year old water ditch. We pinpointed the best location for archaeologists to dig. Later, a team led by consulting archaeologists R. Paul Hampson and C. A. Simpson-Smith uncovered a buried rock pathway. The buried rocks were covered by 17 cm or more of damp sod at the recently watered Mission Plaza in Santa Cruz, California. The buried rock pathway was alongside of the remains of the disturbed water ditch.[3]

The archaeologists believed that a nearby parking lot site covered the remains of the Santa Cruz Mission cemetery. Their belief was based in part on the results of a ground penetrating radar survey conducted by L. Dolphin and T. Yetter at SRI International. A map in Figure 2 shows the site of this survey.

We used available dual band IR scanners elevated 1 to 8 m to interfuse the results of our dual-channel IR methodology with those of the GPR survey. We recorded (on video tape) thermal images showing fourteen long parallel trenches, a cemetery wall and the western extension of the buried "Lost Adobe" barracks (siltstone) foundation first uncovered by archaeologists at a soil-covered site adjacent to the modern asphalt parking lot. The archaeologists hypothesized that Indians may have been buried in trenches (approximately 80 cm deep) following the small pox epidemic in 1838. The foundation was about 45 cm thick covered by 30 cm of silty soil beneath the asphalt. See Figure 2.

We studied a sensor interfusion approach which uses an active IR CO_2 laser reflectance channel. This methodology reduces false alarms generated by surface objects (e.g. rocks, manmade targets or vegetation) at night when photographic methods are ineffective. Laser speckle patterns for aluminum and plastic discs are compared with thermal patterns for a buried inert mine target in Figure 3.

2.0 DEMONSTRATION

The temperature evaluated mapping (TEM) sensor fusion technique is a sensitive, rapid, effective airborne tool developed by the Lawrence Livermore National Laboratory under a Countermine Program Contract with DARPA/BRDEC. This technique is expected to map the sites, pattern and extent of shallow buried land mines. It creates images based on surface temperature variations of 0.2°C. The patented dual-band infrared detection method[4] has two major advantages over other less sensitive detection methods. It detects surface temperature patterns of conducted heat from shallow buried mines which heat and cool at different rates than the surrounding materials. It also removes surface reflectance patterns from rocks, vegetation and metallic objects.

The TEM technology uses a quantitative dual-channel thermal infrared approach. This patented method has been previously used to detect weak heat flow anomalies which produced subtle surface temperature difference patterns of 0.2°C.[2] LLNL used two thermal infrared (IR) bands (near 5 microns and 10 microns) to map true (corrected) surface temperatures. These corrections are described below. This dual-channel method allows us to separate objects with surface temperature

difference patterns from objects with surface reflectance difference patterns. Thus, it is possible to distinguish buried mines from surface rocks or metallic objects. LLNL has adopted this approach to locate shallow buried land mines.

Other less sensitive approaches use one or more radiometric bands to map surface reflectance differences for mineral signature information[5] or to map thermal inertia differences for rock type discrimination.[6] The potential effectiveness of these qualitative thermal approaches applied to land mine detection is tenuous at best. Emissivity-related noise (typically 1°C or 2°C) cannot be removed by the use of one passive thermal IR band in conjunction with another active laser reflectance IR band. By way of contrast, the TEM unique approach uses two passive thermal IR bands thereby allowing subtraction of spatially dependent surface-emissivity noise by decoupling temperature from emissivity effects. TEM detects two IR bands, concurrently, to separate the thermal from the non-thermal components of the IR scanner signals. This method corrects the recorded signals for air path, emissivity and reflected sky radiation effects.[2,7]

The first of four corrections applied to the recorded IR scanner data at filtered wavelengths centered near 5 and 10 microns is a correction to adjust the radiometric (brightness) data at both 5 and 10 microns for the ambient background. The second correction is made to apply the non-linear relationship between the signal intensities and the surface temperatures. This relationship obeys a power law. The radiant emittance is proportional to the emissivity times the absolute temperature to the power of (50/wavelength in microns).[7] The power law thermal model (see Appendix 1) is used to determine signal ratios which are needed to remove surface emissivity noise. The third correction is made to account for the effects of air-path absorption of the infrared signals representing the surface temperature and reemission of the infrared signals representing the mean air-path temperature. A triparameter atmospheric model is used to correct the dual - channel radiometric temperatures.[8] The fourth correction is made for the effects of reflected sky radiation. This correction is proportional to $(1 - \varepsilon) / \varepsilon$ times the recorded temperature minus the sky temperature, where ε is the surface emissivity. Scaled histograms may be useful under certain conditions and for certain surface materials to simplify the procedure for deriving true surface temperatures.

Appropriately scaled (and corrected) 5 and 10 micron imagery of greybody surfaces look alike.[1,2] See Figure 1. Specular surfaces with emissivity differences at 5 and 10 microns do not. By squaring the 10 micron imagery, and dividing by the 5 micron imagery, temperature variations are to a large extent cancelled out and emissivity variations are enhanced. A scrutiny of computer-processed ratioed and differenced imagery is useful for interpreting the origin of thermal or emissivity-related effects.

Grids consisting of two dozen buried mine simulants were set up at three sites for field and helicopter TEM passive dual-band thermal infrared demonstrations (1, 3, 8, 60 and 120 m range). Laboratory and field measurements were used to characterize the thermal diffusivities and conductivities of various soils and buried object filler materials. Fifteen environmental parameters were measured (or estimated) to apply the Annual Temperature Wave Model [7] for predicting surface temperatures for

buried mine sites and nearby surrounding materials. See Appendix 2. TEM proof-of-concept demonstrations produced the first surface temperature images of buried mine simulants (l to 8 m range).[9]

A Daedalus dual-band line scanner was flown by EG&G at Nellis Air Force Base for TEM demonstrations from a helicopter platform (60 and 120 m range). The thermal diffusivity differences between buried mine simulants and their surroundings (not the thermal inertia differences) are considered essential for producing surface thermal images of buried objects. The effects of these thermal diffusivity differences in conjunction with the retained heat of the buried objects and surrounding materials varied with the survey times and conditions. Realtime surface temperature images of various buried mine simulant sites within a grid (25 feet on a side, with 25 grid squares) were recorded with the Agema dual-band image scanner (1 to 8 m range) in connection with the helicopter overflights.

Dual-band signal ratios (and also signal differences) were used to distinguish temperature from surface emissivity noise effects on the resulting thermal imagery collected at (unfiltered) wavelengths centered near 5 and 10 microns. It was difficult to determine the appropriate scaling factor to simplify interpretation of the true surface temperatures, since the rented scanner spectral calibrations were not available. Subsequently, we have obtained the Agema 12-bit digital, 880 dual system and are calibrating and optimizing spectral responses needed for TEM demonstrations from field or helicopter platforms. This instrumentation will provide realtime scaling and signal differences needed to distinguish temperature from surface emissivity noise effects greatly simplifying interpretation of thermal images.

The results of the helicopter platform TEM thermal imagery showed some evidence indicating symmetric heating and cooling of materials surrounding buried land mine simulants which effectively enlarged their respective surface temperature "footprints". The wind direction, heat transfer and re-radiation from bushes produced thermal plumes on their respective leeward side, a natural thermal effect unrelated to buried objects. Surface mine simulants recorded with the dual-band scanner before sunrise had halos (warm rings) from re-radiation off edges (8 to 10 cm high) to the surrounding dry sand.

Precise surface temperatures were recorded every 5 minutes at 17 sites (e.g., dry sand, wet sand and wet grassy sod, with and without buried mine simulants) using vertical and horizontal thermistor probes and grid arrays calibrated to within 0.2°C. These measurements were made before, during and after the helicopter overflights, on cloudy and clear days, to test the Annual Temperature Wave Model predictions and calibration procedures for deriving true surface temperature maps. See Figures 4, 5 and 6 and Appendix 2. Strong winds and heavy cloud cover are to be avoided since they have a tendency to mask surface temperature "footprints" from buried objects. Also, shading at low sun angles after sunrise and before sunset makes interpretation difficult.

Buried and surface land mine simulants were observed to have thermal, spectral, spatial, emissivity and temporal signatures. Thermal mine simulants received from INEL were buried with a grid of 25 buried mine simulants (e.g., plastic filled with

paste, epoxy resin, dry sand, wet sand and nylon-wax, PVC and metal filled with epoxy resin) at depths of 1, 5, 10, and 15 cm. The INEL simulants (row three, columns two, three and four) at respective depths of 1, 5 and 10 cm under dry sand were observed with the corrected thermal imagery. See Figures 7-11. The nylon-wax filled plastic-mine-simulant thermal response was seen off center of the grid square and subsequently discovered to be buried off center. This simulant was buried 10 cm deep. Calculations imply it lowered the surface temperature less than 0.5°C during the overflight at 1849 hours PDT.

The conditions predicted to have optimum thermal discrimination on September 27 (at 1245 PDT) had minimal discrimination because of heavy cloud cover and high winds. Surface mines borrowed from WES and other surface targets were placed beneath bushes and under water, wet sand and wet grassy sod. Airborne dual-channel data were recorded simultaneously with thermometric, radiometric, photographic and meteorologic data on this cloudy autumn day at approximately 0545, 1245, and 1845 hours PDT. The minimum detectable surface temperature difference was less than 0.5°C using the available Daedalus 1260 digital scanner previously used to map 0.2°C differences[1,2].

At certain calculable times of day, for various wind velocity and cloud cover conditions, mine simulant thermal "footprints" will differ less than 0.5°C (which is the present detection threshold) from their surroundings. Under these conditions, the ground disturbances related to buried or surface mines may (or may not) provide other, less definitive thermal, spectral or spatial indicators of approximate mine positions.

3.0 CONCLUSION

Whereas the military community has developed very impressive single-band passive IR systems,[10] we believe that to site buried land mines, the intrafusion of two passive IR sensors (which exploits Planck's radiation law) will greatly aid interpretation and reduce false alarms. Our goal is to apply a recently developed low thermal noise, dual system digitized IR scanner for buried mine detection and to transition this technology to the military and industrial community. Also, some of the other applications we plan to develop relate to open skies, drug traffic control and environmental restoration at waste burial sites.

4.0 ACKNOWLEDGEMENTS

This work was performed under the auspices of the U.S. Department of Energy by the Lawrence Livermore National Laboratory under contract number W-7405-ENG-48 for the U.S. Department of Defense DARPA/BRDEC Countermine Program, ARPA order number 7180-01. The author acknowledges valuable technical discussions with Tom Hafer (DARPA), Bob Barnard (BRDEC), Paul Duffy (TEXTRON/TDS), Suzanne Lake (LLNL) and Larry Tinney (EG&G/EM); LLNL sponsorship by Milt Finger and Richard Fortner; field operations support by EG&G's David Hawley, Jan Shines, Charles Golanics, Mark McDermot and LLNL's Don Gerigk, Phil Durbin, Merv Lawrence; thermal imagery processing by Ed Doak (EG&G) and Eric Frerking (LLNL); field testing of the CO_2 laser reflectance signatures by Tom Kulp (LLNL); inert mine

simulants from Dan Cress (WES) and Jim Rohrbaugh (INEL); surface temperature simulations by John Lewis at McGill University; and the use of Agema image scanners provided by Mike McGinn, Bill Martin and Phil Smith.

5.0 REFERENCES

1. Del Grande, N. Kerr, "Airborne and Field Temperature Surveys Compared at Long Valley KGRA, California"; in Geothermal Resources Council Transactions 5, p. 71, 1981.

2. Del Grande, N. Kerr, "Airborne Temperature Survey Maps of Heat Flow Anomalies for Exploration Geology"; in Proceedings of International Symposium on Remote Sensing of Environment, Second Thematic Conference on Remote Sensing for Exploration Geology Dec. 1982. Reprinted in Geothermal Resources Council Bulletin 14, p.3, Mar. 1985.

3. Larimer, Tim, "Digging into city's past, archaeologists find Santa Cruz Mission's water ditch"; in San Jose Mercury News, Sunday morning, October 2, 1988.

4. Del Grande, N. K. "Method for Identifying Anomalous Terrestrial Heat Flows"; Patent No. 4,005,289, Jan. 1977.

5. Kahle, A. and Goetz, A., "Mineralogical information from a new airborne thermal infrared multispectral scanner"; in Science 222, p. 24, 1983.

6. Short, N. and Stuart, L. The Heat Capacity Mapping Mission (HCMM) Anthology; NASA/GSFC, p. 1-14, 1982.

7. LeSchack, L. A. and Del Grande, N. K. "A Dual-Wavelength Thermal Infrared Scanner as a Potential Airborne Geophysical Exploration Tool"; in Geophysics 41, p. 1318, 1976.

8. LeSchack, L. A., Del Grande, N. K., Lewis, J. and Jenner, C. "Correlation of Dual-Channel Airborne IR Data with Soil Moisture Measurements"; in NOAA/NESS Final Report No. 6-35191 Appendix E, reprinted Feb. 1978.

9. Del Grande, N. "Temperature Evaluated Mine Position Survey (TEMPS) Application of dual-Band Infrared Methodology"; in Proceedings of the 1990 Meeting of the IRIS Specialty Group on Passive Sensors; IRIA/ERIM-sponsored symposium, March 1990.

10. Nettleton, D. and Groenwald, R. "AMIDARS flight performance"; in SPIE Vol. 979 Airborne Reconnaissance XII, p. 8, 1988.

Appendix 1

1.0 DERIVATION OF POWER-LAW THERMAL MODEL [7]

The spectral radiant emittance W_λ, measured in units of (watts/m²)/unit wavelength, is what is detected by an airborne ir scanning system. Planck's equation expresses W_λ as follows:

where $W_\lambda = \epsilon_\lambda C_1 \lambda^{-5}[\exp(C_2/\lambda T) - 1]^{-1}$. A-1

ϵ_λ = surface emissivity at a given wavelength λ,
$C_1 = 3.7414 \times 10^8\ W/m^2 \cdot \mu m^4$,
$C_2 = 1.4388 \times 10^4\ \mu m \cdot K$,
λ = wavelength in μm,
T = surface temperature in K.

Since the scanner senses not the entire range of emitted energy but only that energy contained in the wavelength band for which the system is designed, equation (A-1) should be expressed as

$$W = \int_{\lambda_1}^{\lambda_2} \epsilon_\lambda C_1 \cdot [\exp(C_2/\lambda T) - 1]^{-1}\lambda^{-5}\, d\lambda. \qquad \text{(A-2)}$$

To simplify the mathematics, we will make the following substitution:

$$y = C_2/\lambda T, \qquad \text{(A-3)}$$

and, therefore, it follows that $\lambda = C_2/Ty$. By differentiating,

$$\lambda^{-5} d\lambda = -C_2^{-4}T^4y^3dy. \qquad \text{(A-4)}$$

Equation (A-2) can now be rewritten

$$W = \int_{y_1}^{y_2} \frac{\epsilon_\lambda C_1}{\exp(y) - 1} \cdot (-C_2^{-4}T^4y^3)\, dy,^7 \qquad \text{(A-5)}$$

or

$$W = -\epsilon_\lambda C_1 C_2^{-4} T^4 \cdot \int_{y_1}^{y_2} \left(\frac{y^3}{\exp(y) - 1}\right) dy. \qquad \text{(A-6)}$$

Multiplying the numerator and denominator of the bracketed term by $(\exp -y)$, we have

$$\frac{y^3 \exp(-y)}{1 - \exp(-y)},$$

and

$$W = -\epsilon_\lambda C_1 C_2^{-4} T^4 \cdot \int_{y_1}^{y_2} \left(\frac{y^3 \exp(-y)}{1 - \exp(-y)}\right) dy. \qquad \text{(A-7)}$$

The term

$$\frac{\exp(-y)}{1 - \exp(-y)}$$

can be expanded in a binomial series, as

$$\exp^{-y} \sum_{m=0}^{\infty} \exp(-my) = \exp(-y)[\exp(-0) + \exp(-y) + \exp(-2y) + \cdots \exp(-my)]$$

or

$$[\exp(-y) + \exp(-2y) + \exp(-3y) + \cdots \exp -(m+1)y]$$

which can be expressed as

$$\sum_{m=1}^{\infty} \exp(-my).$$

Equation (A-7) can now be rewritten using the above expansion and eliminating the negative sign by reversing the limits of integration as follows:

$$W = \epsilon_\lambda C_1 C_2^{-4} T^4 \cdot \int_{y_1}^{y_2} y^3 \left(\sum_{m=1}^{\infty} \exp(-my)\right) dy. \qquad \text{(A-8)}$$

Integrating equation (A-8) by parts, using the form

$$\int y^3 \exp(-my)\, dy = \frac{y^3 \exp(-my)}{-m} - \frac{3}{-m}\int y^2 \exp(-my)\, dy,^8$$

we obtain

$$W = \epsilon_\lambda C_1 C_2^{-4} T^4 \cdot \left[\sum_{m=1}^{\infty} \exp(-my_2)\left(\frac{y_2^3}{m} + \frac{3y_2^2}{m^2} + \frac{6y_2}{m^3} + \frac{6}{m^4}\right) - \sum_{m=1}^{\infty} \exp(-my_1) \cdot \left(\frac{y_1^3}{m} + \frac{3y_1^2}{m^2} + \frac{6y_1}{m^3} + \frac{6}{m^4}\right)\right]. \qquad \text{(A-9)}$$

[7] For integrations over small wavelength intervals, ϵ_λ is considered constant; λ applies to the mean wavelength.

[8] Standard Mathematical Tables, Chemical Rubber Company, 12th Ed., 1962, p. 309, Integral #354.

Equation (A-9) is a complete expansion of Planck's equation. However, it is unwieldy to evaluate for our emissivity ratio analysis.

Accordingly, we have derived an approximation of equation (A-9) that considerably simplifies the mathematics. Differentiating equation (A-1) with respect to T and holding λ constant, we obtain

$$dW_\lambda = \epsilon_\lambda C_1 \lambda^{-5} \cdot \frac{(C_2/\lambda T^2)\exp(C_2/\lambda T)}{(\exp(C_2/\lambda T) - 1)^2}\, dT. \qquad \text{(A-10)}$$

Dividing equation (A-10) by W_λ, we obtain

$$\frac{dW_\lambda}{W_\lambda} = \frac{(C_2/\lambda T^2)\exp(C_2/\lambda T)}{[\exp(C_2/\lambda T) - 1]}\, dT, \qquad \text{(A-11)}$$

or

$$\frac{dW_\lambda}{W_\lambda} = (C_2/\lambda T) \cdot \left[\frac{\exp(C_2/\lambda T)}{\exp(C_2/\lambda T) - 1}\right]\frac{dT}{T}. \qquad \text{(A-12)}$$

The bracketed term, by multiplying and dividing by $\exp(-C_2/\lambda T)$, can be rewritten

$$\left[\frac{1}{1 - \exp(-C_2/\lambda T)}\right],$$

which is of the form $1/1 - x$, where $x = \exp(-C_2/\lambda T)$. It therefore can be expressed as a binomial expansion of the form

$$\frac{1}{1-x} = 1 + x + x^2 + \cdots x^m = \sum_{m=0}^{\infty} x^m,$$

as long as $\exp(-C_2/\lambda T) < 1$. This will be the case for the wavelengths of interest in this work. With the nominal temperature of 15°C or 288 K (recorded at the time of the field study) and for data recorded in wavelengths less than 15 μm, the bracketed term is approximately equal to unity; this is because the second and higher order terms of the expansion are much less than 1.

Accordingly, Equation (1-12) can be expressed as

$$\frac{dW_\lambda}{W_\lambda} = \frac{C_2}{\lambda T}\frac{dT}{T}. \qquad \text{(A-13)}$$

Since by definition, $dW_\lambda/W_\lambda = d\ln W_\lambda$, and $dT/T = d\ln T$, for small temperature excursions less than ±5 K from T_0, where $T = T_0(1 \pm \Delta T/T_0) \cong T_0$, integrating equation (A-13) becomes:

$$\ln W_\lambda \Big|_{W_\lambda(T_0)}^{W_\lambda(T)} = -\frac{C_2}{\lambda}\cdot\frac{1}{T}\Big|_{T_0}^{T}, \qquad \text{(A-14)}$$

$$\ln \frac{W_\lambda(T)}{W_\lambda(T_0)} = -\frac{C_2}{\lambda}\left(\frac{1}{T} - \frac{1}{T_0}\right) = -\frac{C_2}{\lambda T_0}\left(\frac{T_0}{T} - 1\right), \qquad \text{(A-15)}$$

whence

$$W_\lambda(T) = W_\lambda(T_0)\exp\left(\frac{T_0}{T} - 1\right) \cdot \left(-\frac{C_2}{\lambda T_0}\right) \qquad \text{(A-16)}$$

$$= W_\lambda(T_0)\left[\exp\left(\frac{T_0}{T} - 1\right)\right]^{-C_2/\lambda T_0} \qquad \text{(A-17)}$$

Since T is near T_0, $(T_0/T - 1)$ is small, and we may expand the exponential obtaining

$$W_\lambda(T) = W_\lambda(T_0)\left[1 + \left(\frac{T_0}{T} - 1\right)\right]^{-C_2/\lambda T_0}, \qquad \text{(A-18)}$$

$$= W_\lambda(T_0)\left(\frac{T_0}{T}\right)^{-C_2/\lambda T_0}$$

$$= W_\lambda(T_0)\left[\frac{T}{T_0}\right]^{C_2/\lambda T_0} \qquad \text{(A-19)}$$

$$= \frac{W_\lambda(T_0)}{T_0^{(C_2/\lambda T_0)}}\cdot T^{(C_2/\lambda T_0)} \qquad \text{(A-20)}$$

$$= C_\lambda(T_0)T^{(C_2/\lambda T_0)} \propto \epsilon_\lambda T^{(C_2/\lambda T_0)}. \qquad \text{(A-21)}$$

For $C_2 = 14{,}388\ \mu\text{m} \cdot \text{K}$ and a nominal value of $T_0 = 288$ K, $C_2/T = 49.96$, equation (21) can be closely approximated by

$$W_\lambda \propto \epsilon_\lambda T^{50/\lambda}. \qquad \text{(A-22)}$$

We have computed the difference for a change of W_λ from $T = 288$ K to $T = 289$ K by evaluating equation (A-9), the complete expansion of Planck's equation, and Equation (A-22). Comparing the results, we found that for the wavelengths of interest to us (i.e., between 5 μm and 15 μm), equation (A-22) introduces an error of no more than ± 0.04 percent. From the above, we have derived a convenient expression relating the radiant emittance sensed by a typical *ir* scanner to the absolute surface temperature raised to the power of $50/\lambda$. This power law thermal model becomes an extremely useful mechanism for enhancing either the effects of emissivity or of surface temperature.

Appendix 2

1.0 ANNUAL TEMPERATURE WAVE MODEL

Based on the energy conservation equation, S.I. Outcalt developed a model described previously for simulating the surface temperature.[7] This model was adapted by John E. Lewis, Jr. at McGill University to predict surface temperature changes from buried mine simulants at depths of 1, 5, 10 and 15 cm. It is described below.

Table 1. Environmental Input Parameters

Station pressure (P)	Sky radiant temperature (TSKY)
Latitude (LAT)	Mean air temperature (TA)
Solar declination (DEC)	Mean air relative humidity (RH)
Dust particles (D)	Mean wind speed (U)
Orbital radius vector (R)	Soil thermal diffusivity (GD)
Surface Albedo (ALBEDO)	Soil volumetric heat capacity (GC)
Precipitable water (W)	Soil surface wetness (SRH)
Surface Roughness length (ZO)	

The model solves the energy conservation equation. The net radiation R, soil heat flux S, sensible heat flux H, and latent heat flux L must have a zero sum across a surface:

$$R + S + H + L = 0. \qquad (1)$$

These terms are expressed as complex functions of the environmental variables and the only unknown which is the surface temperature T, as

$$R = f\,(LAT, DEC, D, R, ALBEDO, W, P, TSKY, T). \qquad (2)$$

Given that the soil temperature at the diurnal damping depth is approximately equal to the mean air temperature, it follows that

$$S = f\,(GC, GD, TA, T). \qquad (3)$$

Turbulent transfer terms (corrected for stability using the Richardson number) are expressed as:

$$H = f\,(U, ZO, P, TA, T), \qquad (4)$$

$$L = f\,(U, ZO, P, RH, SRH, TA, T). \qquad (5)$$

The model solves the finite-differences form of the soil thermal diffusivity equation. The output of this model is the absolute temperature as a function of solar time for each survey point.

Modifications of this model were made to simulate surface temperature variations with and without subsurface materials at various depths which have different heating and cooling rates than the surrounding materials at different survey times and months.

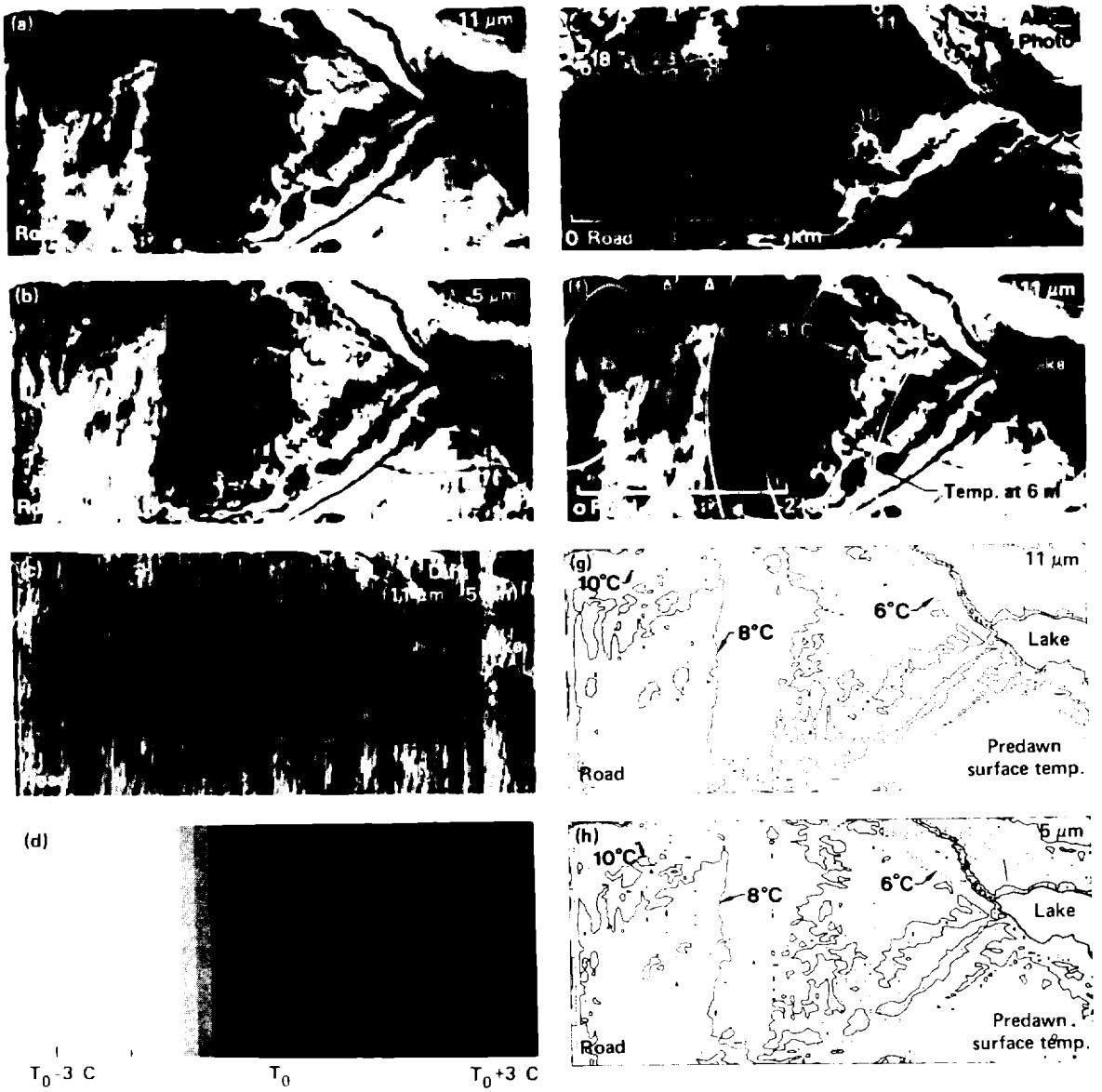

Figure 1. Corrected predawn radiometric temperatures at 11 microns (a), 5 microns (b), and the subtracted temperature difference (c), calibrated at 0.2°C intervals (d), and compared with aerial photo (e), 6-m-deep temperature contours (f), and surface predawn temperature contours at 11 microns (g) and 5 microns (h).[1] Note 8°C aquifer contour.

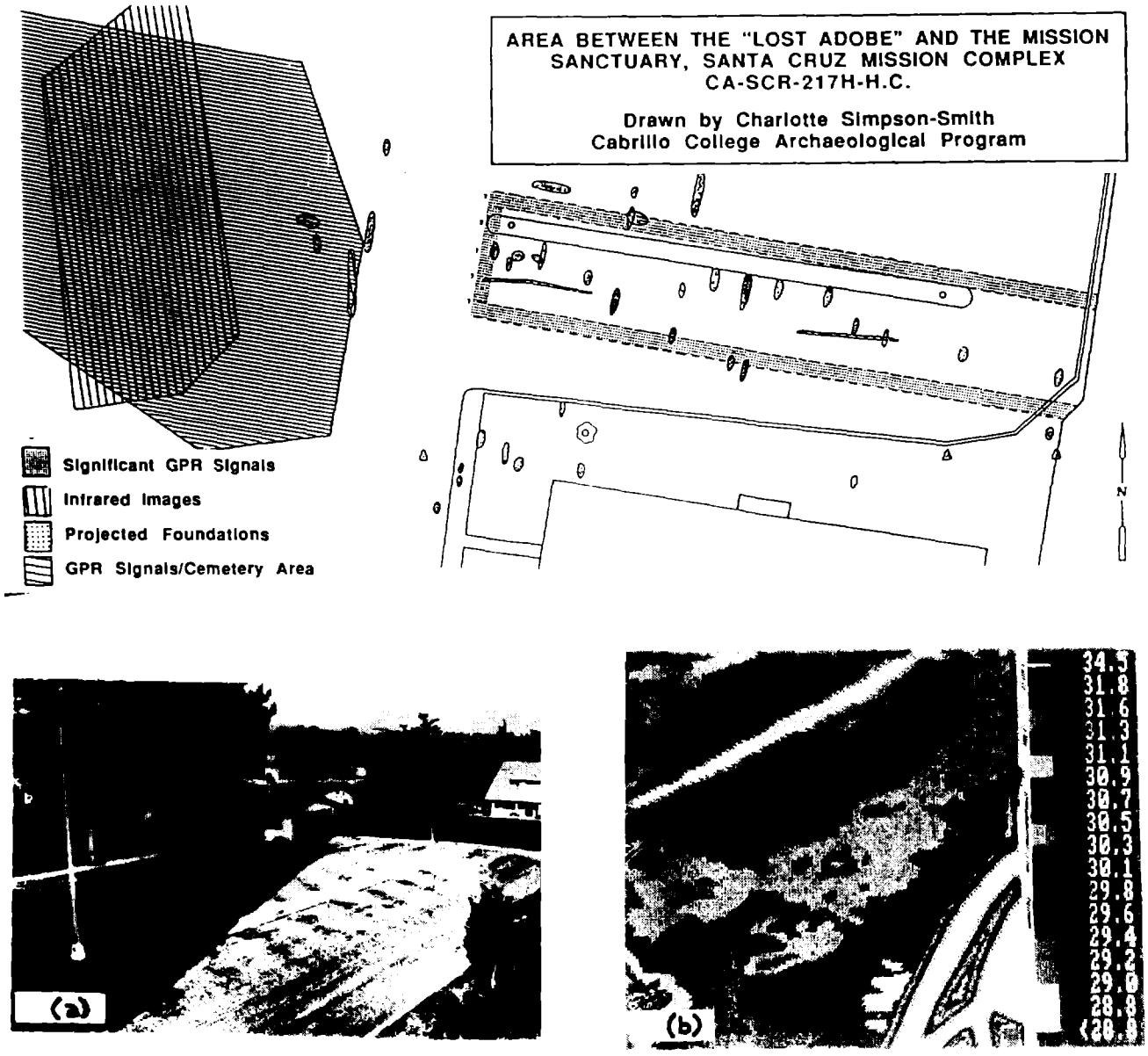

Figure 2. Map of Mission Hill parking lot covered by asphalt pavement where ground penetrating radar (GPR), photographic and IR surveys were conducted. Photo in (a) shows area east of buried cemetery site and adjacent to unpaved (backyard) site where Indian barracks foundation was discovered. Thermal image in (b) at the center of the photographed area shown in (a) depicts southwest corner of the siltstone foundation (see rectangle) which is less than 0.5°C colder than the surrounding areas to the south which overlay silt.

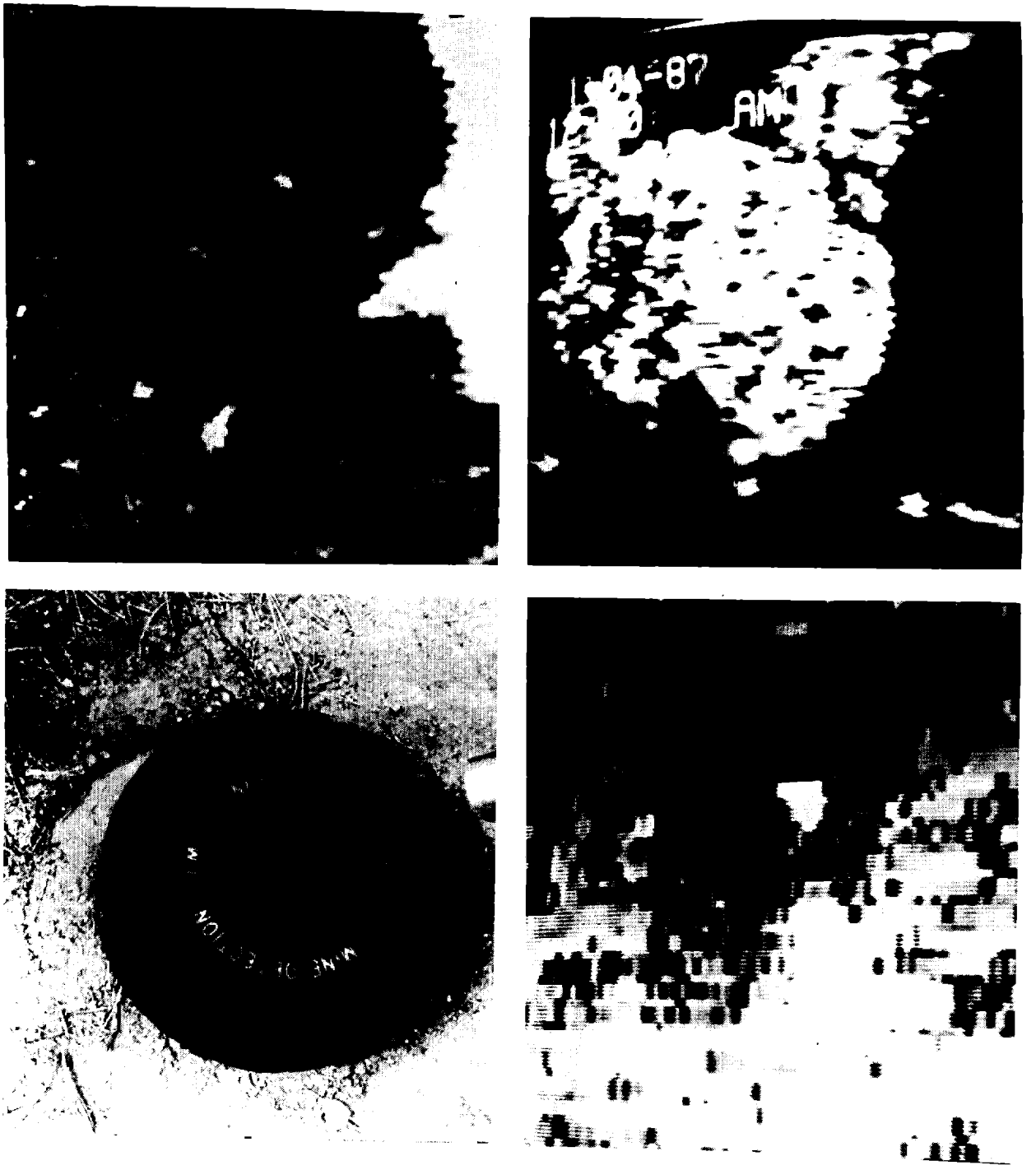

Figure 3. At top left, a person is standing next to a 10 inch diameter plastic disc placed on the ground. With active IR (CO_2 laser) reflectance at a slant angle, the surface target appears mostly black. At top right, a hand-held 12 inch diameter aluminum disc appears bright when laser light at 10.6 microns is reflected perpendicular to the surface. At bottom left, the photo shows an inert mine target. At bottom right (looking downward), the black image is a cool thermal "footprint" above a buried inert mine target surrounded by sand. Note the warm (white) surface rock which masks part of this image and the surface metallic marker placed above and to the left of it.

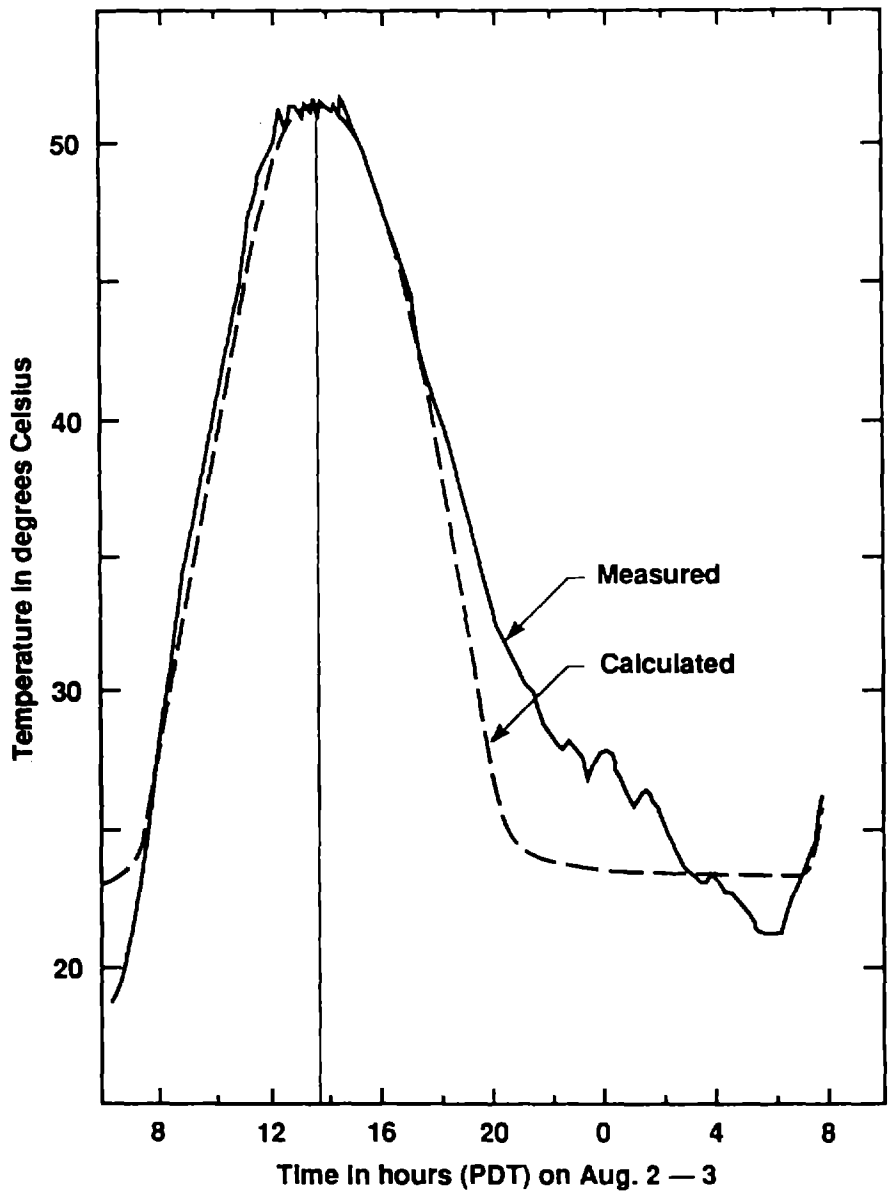

Figure 4. Surface temperature predictions versus measurements which tested the Annual Temperature Wave Model.[7]

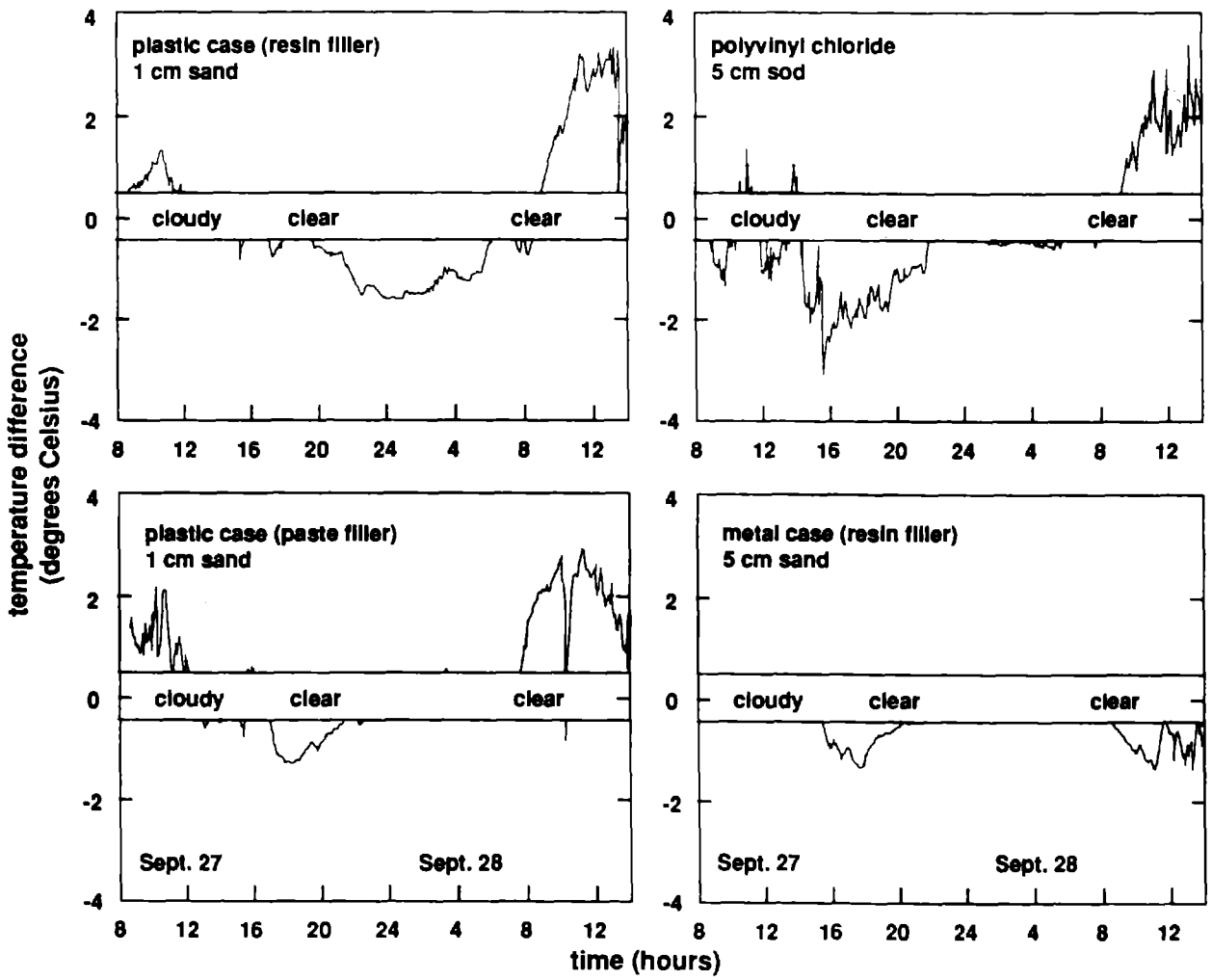

Figure 5. Recorded surface temperature change directly above four buried mine simulants during Nellis AFB overflights, Sept. 27 at 12:45 and 18:49 PDT.

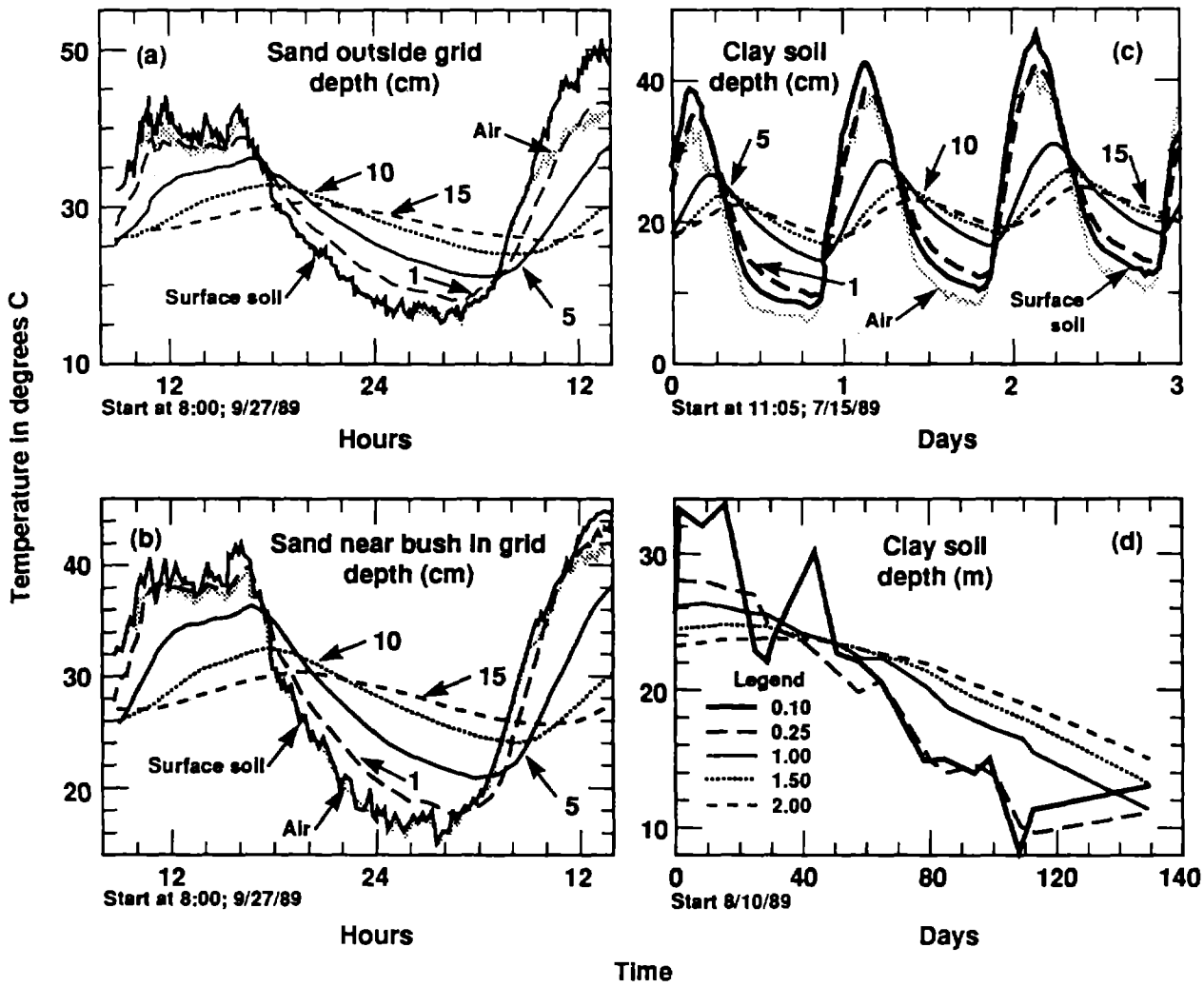

Figure 6. Day-night temperature changes at 0 to 15 cm depths (a, b, c) and seasonal temperature changes at 0.1 to 2 m depths (d).

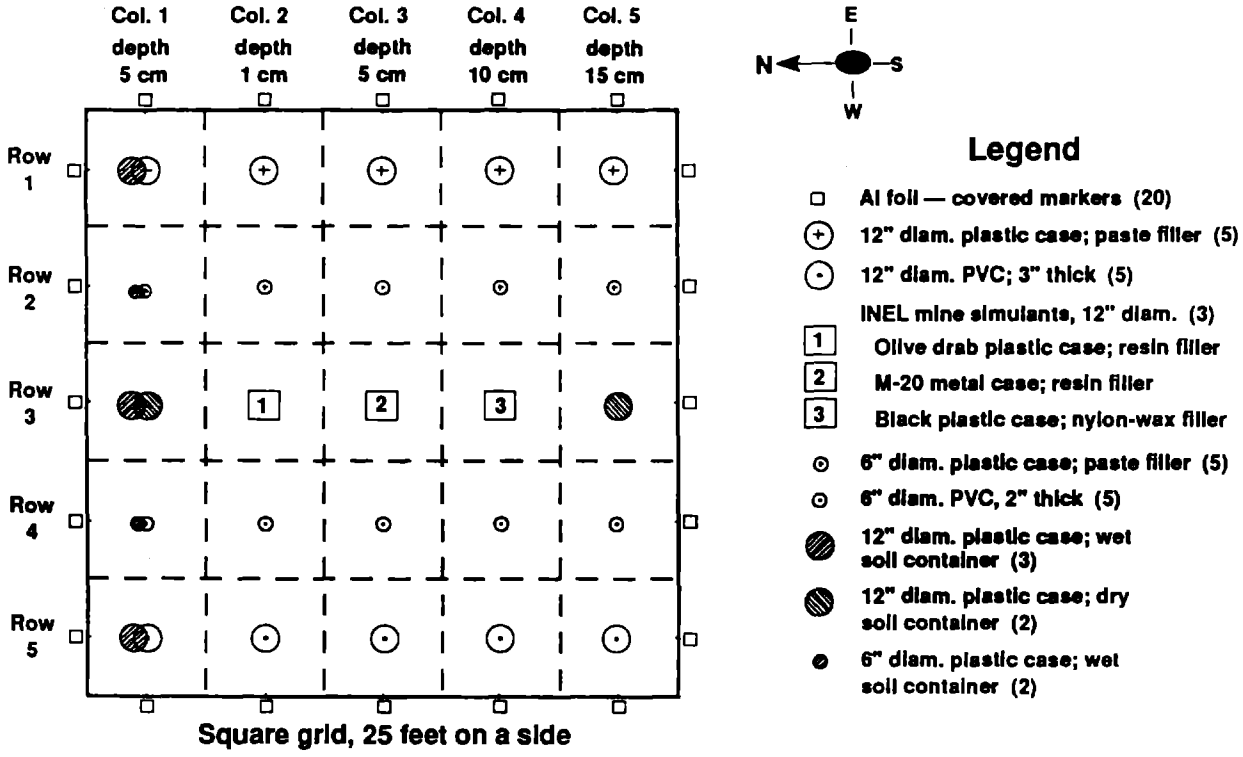

Figure 7. Nellis Air Force Base buried mine simulant grid layout.

Figure 8. Nellis Air Force Base TEM grid site. Top southwestern view shows 12-inch diameter surface mine simulants north of rows 1, 3 and 5. Bottom northern view shows two water baths; 12-inch diameter surface mine simulants near bush at bottom left; sod south of row 3; bush within grid (row 2, column 3); and fence alongside of row 1.

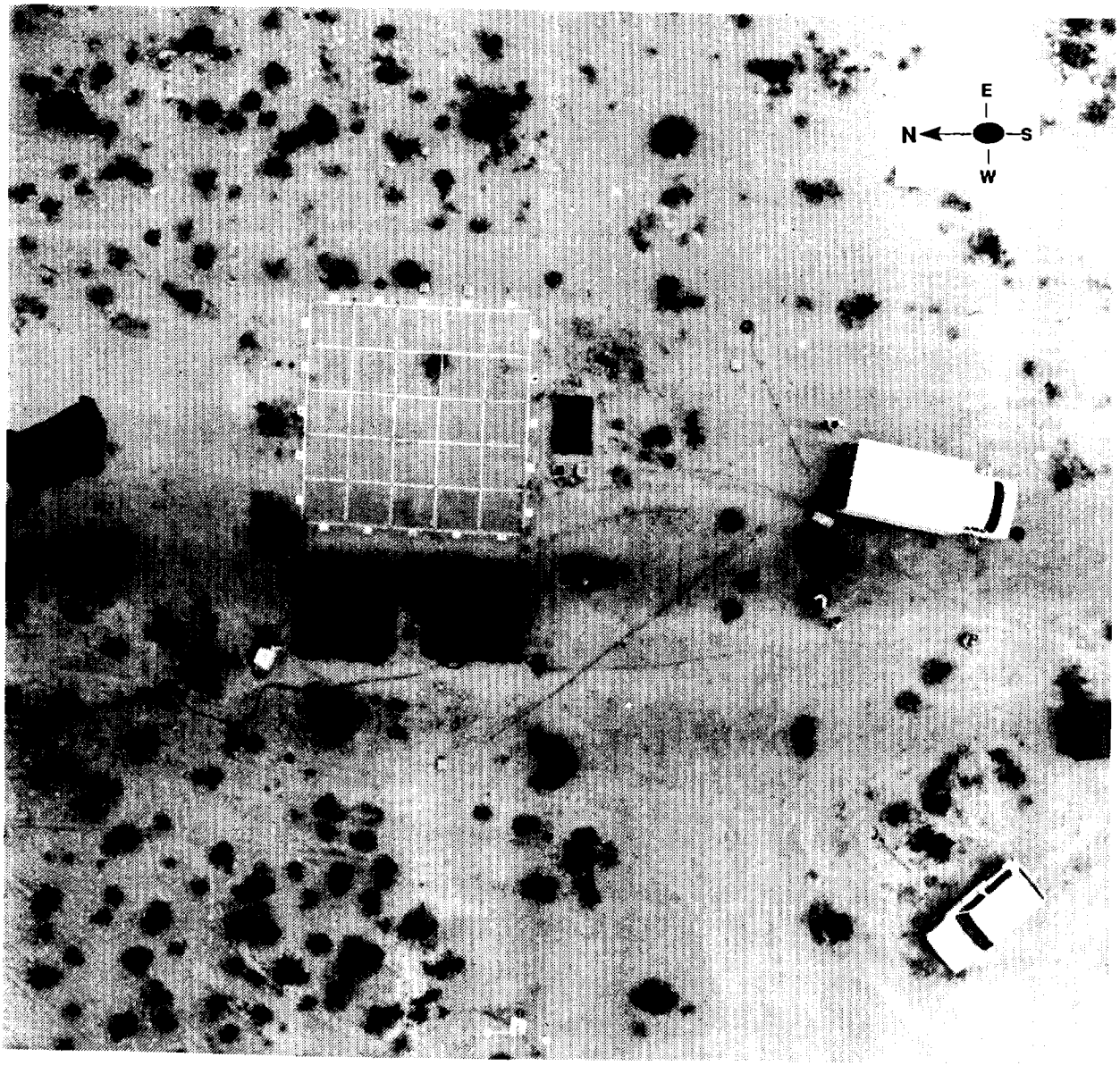

Figure 9. Helicopter overview of TEM burial site mine detection grid taken at an elevation of 60 meters at Nellis AFB.

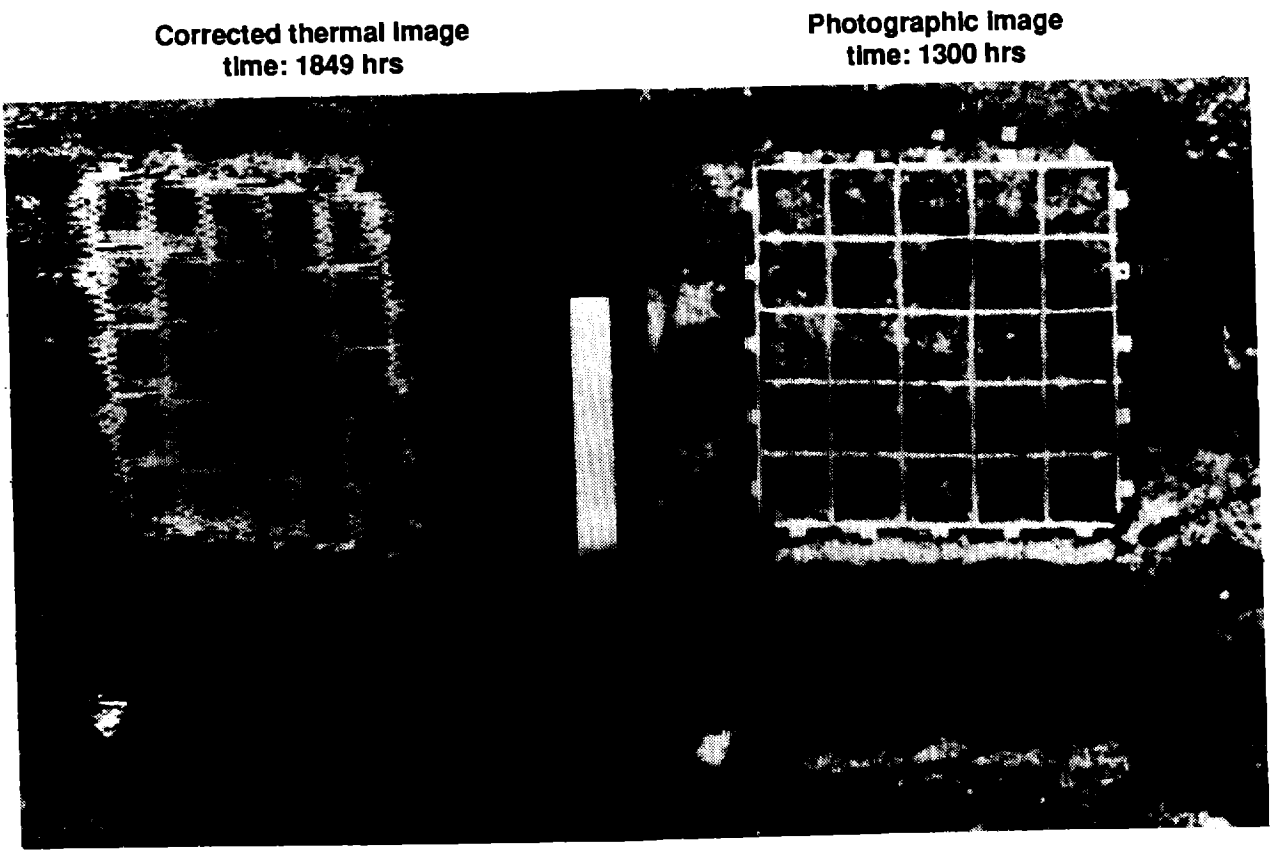

Figure 10. Nellis AFB burial site mine detection grid (viewed from helicopter at 60 meters). The minimum resolvable thermal "footprint" produced less than a 0.5°C surface temperature drop from a 10-cm-deep buried mine simulant at 1849 hours on Sept. 27. Note off-center grey (cooler) zone at row 3, column 4. Note also the different patterns on the photographic image from those seen on the thermal image. Both images were derived from digital data.

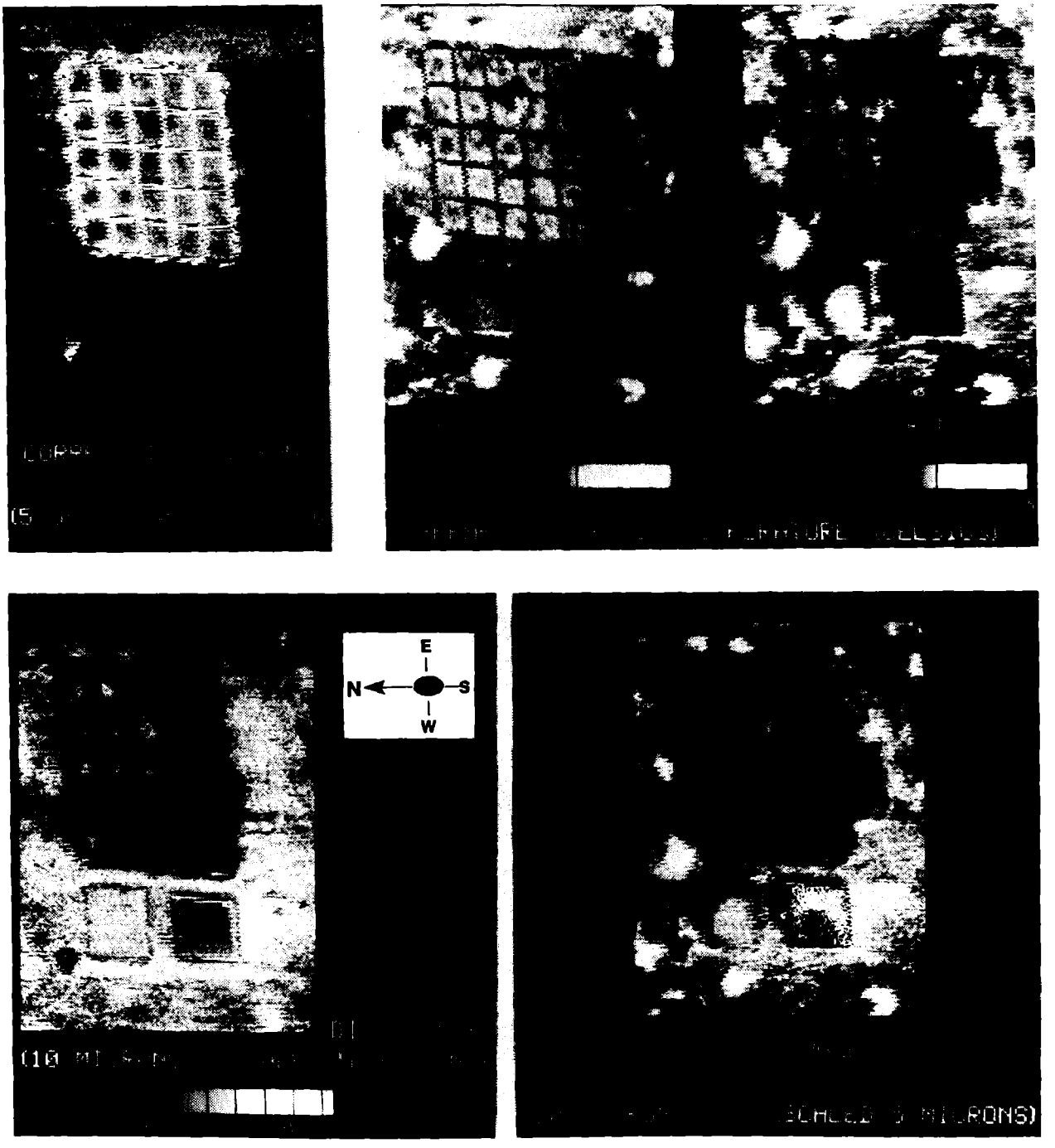

Figure 11. TEM burial site mine detection grid at Nellis AFB showing differences (within grid) of upper thermal "footprint" signatures and lower emissivity-related signatures. The corrected (5 micron) buried target thermal "footprints" were cooler than their surroundings, whereas the surface target thermal "footprints" were warmer than their surroundings at 1849 hours on September 27 (just north and southwest of grid). These temporal effects were predicted by the Annual Temperature Wave Model (see Appendix 2).